

Radiation conditions for the time-dependent Schrödinger equation: Application to strong-field photoionization

K. Boucke and H. Schmitz*

Lehrstuhl für Lasertechnik, Steinbachstrasse 15, Rheinisch Westfälische Technische Hochschule, D-52074 Aachen, Germany

H.-J. Kull

Institut für Theoretische Physik A, Rheinisch Westfälische Technische Hochschule, D-52056 Aachen, Germany

(Received 17 May 1996; revised manuscript received 13 January 1997)

Radiation conditions are introduced as an exact method to truncate numerical solutions of the time-dependent Schrödinger-equation at the boundaries of the numerical grid. A rigorous derivation of radiation conditions is given by the Green-function method for one- and three-dimensional regions. An accurate finite-difference representation is obtained for a one-dimensional region. The method is applied to calculations of strong-field photoionization. The calculation of ionization probabilities and energy spectra by the truncated solution is illustrated. [S1050-2947(97)06107-6]

PACS number(s): 32.80.Rm, 31.15.-p

I. INTRODUCTION

Over the past decade, the numerical solution of the time-dependent Schrödinger equation (TDSE) has received broad attention in the study of atomic and molecular systems. In particular, there have been great advances in the treatment of atoms in strong radiation fields [1], demonstrating various nonperturbative phenomena, e.g., in above-threshold ionization (ATI) [2] and optical harmonic generation [3]. While most previous computations have been based on one-dimensional model atoms [4–9], more realistic multidimensional atoms have been successfully treated in some cases [10–13]. Numerical TDSE calculations also offer a valuable complement to Floquet methods otherwise widely used in atomic physics [14].

In this work, an exact method is presented to truncate numerical solutions of the TDSE at the boundaries of the numerical grid. It is our principal goal to demonstrate the computational efficiency and accuracy of this method for calculations of strong-field photoionization. For simplicity, the present calculations have been limited to a one-dimensional model atom, although future three-dimensional extensions appear conceivable.

The present approach is based on exact boundary conditions for outward propagating solutions of the TDSE. In analogy with the theory of electromagnetic waves, these boundary conditions will be called radiation conditions [15]. While radiation conditions are commonly used for monochromatic waves, their general form for an arbitrary time-dependent solution on an arbitrarily shaped boundary seems less well understood. The general boundary condition constitutes a linear relationship between boundary values, which is nonlocal in space and time. The derivation of the appropriate propagator and of an accurate discretization scheme repre-

sent the basic problems to be solved for computational applications.

In previous work, boundary reflections have often been recognized as a crucial limitation in TDSE calculations. If simple *ad hoc* (e.g., rigid, periodic) boundary conditions are chosen, the wave function is reflected at the boundaries, causing an unphysical feedback to the system. For computational convenience, one therefore often needs to truncate the wave function in the asymptotic region. One of the standard truncation procedures is based on absorbing diffuse boundaries. Absorbing boundaries have been modeled by various types of imaginary-valued potentials [4,16–18]. Particularly accurate results have been obtained for a properly chosen linear absorber function [18]. A related truncation method uses wave-function splitting [19], which propagates the asymptotic and interacting parts of the wave function separately. Both methods are approximate in the sense that a weak variation of parameters in the absorber region is required.

Occasionally, exact truncation methods have also been reported. Exact convergence in the asymptotic region can be achieved by analytic continuation, using complex coordinate contours [20] or complex eigenfunction expansions [21,22]. Boundary conditions similar to those presented here have already been studied in a more mathematical context [23]. However, the method of derivation and the final discretization schemes are different. The present approach is based on Green functions, and the discrete representation is obtained by removing a singularity from the kernel before making finite-difference approximations. Apparently, the applicability of radiation conditions to atoms interacting strongly with an electromagnetic field has not been addressed before.

In Sec. II, a general background is presented, showing how radiation conditions for the TDSE can be derived analytically by the Green-function method. This method applies equally well to a large class of partial differential equations, including parabolic, hyperbolic, and elliptic equations [24]. The use of radiation conditions in numerical computations therefore may be of general interest in diverse fields. An

*Present address: Max-Planck-Institut für Polymerforschung, Postfach 3148, D-55021 Mainz, Germany.

accurate finite-difference representation of these boundary conditions can be obtained in the one-dimensional case, which represents the principle result of this work.

In Sec. III, the numerical method is applied to TDSE calculations of photoionization. Thereby the accuracy of the method is demonstrated by comparison with the full solution, and furthermore, explicit calculations of ionization probabilities and energy spectra are presented. Atomic units will be used throughout this paper.

II. RADIATION CONDITIONS

Radiative boundary conditions are commonly introduced in the frequency-momentum domain, where ingoing and outgoing waves, propagating along a particular direction, can simply be distinguished by the sign of the group velocity. However, this criterion is not immediately applicable to numerical computations in the space-time domain. Therefore, in this section, radiation conditions will directly be introduced in the space-time domain by using the Green-function method. The problem of specifying an outward propagating solution by boundary values can be reduced to the determination of a particular Green function for the region, exterior to the boundary. The general method will be demonstrated in the following by considering the specific case of the free-particle TDSE. The corresponding Green function will be explicitly calculated for a one-dimensional half-space and for the region exterior to a three-dimensional sphere. The one-dimensional result will be further reduced to a finite-difference expression for computational applications.

A. Green-function method

Consider a spatial region R enclosed by a surface S where radiative boundary conditions are required. Let $\psi(\mathbf{x}, t)$ denote the wave function of an electron, which is localized initially, at time $t=0$, within R but may propagate outward through the surface S into the exterior region for times $t>0$. Specifically, we will assume that the propagation in the exterior region is governed by the free-particle TDSE,

$$L(\mathbf{x}, t)\psi(\mathbf{x}, t) = 0, \quad L(\mathbf{x}, t) = i\partial_t + \frac{1}{2}\Delta. \quad (2.1)$$

The exterior solution can be completely determined in terms of boundary values for either the wave function or its normal derivative on S . These boundary values will be denoted as

$$\psi(\mathbf{x}, t)|_S = f(\mathbf{x}_s, t), \quad \partial_n \psi(\mathbf{x}, t)|_S = g(\mathbf{x}_s, t), \quad (2.2)$$

respectively, where $\partial_n = \mathbf{n} \cdot \nabla$ denotes the normal derivative on S . The surface normal unit vector \mathbf{n} is taken directed from the surface S toward the exterior region. If, for instance, $g(\mathbf{x}_s, t)$ is prescribed, $f(\mathbf{x}_s, t)$ will be determined by the solution of Eq. (2.1) subject to the outgoing wave conditions

$$\psi(\mathbf{x}, 0) = 0, \quad \psi(\mathbf{x}, t)|_{|\mathbf{x}| \rightarrow \infty} = 0 \quad (2.3)$$

for the external region. The relationship between the boundary values f and g represents the desired boundary condition for the internal region R .

The basic equation for expressing the exterior solution in terms of initial-boundary values is the Lagrange-Green identity of the operator L . It can be derived by multiplying the

left-hand side of Eq. (2.1) by an arbitrary function $K(\mathbf{x}, t)$ and integrating this expression over the volume V of the exterior region and the time interval from $t=0$ up to $t=\infty$. Denoting integration variables by a prime, and performing a number of partial integrations, one finds

$$\begin{aligned} & \int_V dV' \int_0^\infty dt' \{K(\mathbf{x}', t')L(\mathbf{x}', t')\psi(\mathbf{x}', t') \\ & \quad - \psi(\mathbf{x}', t')L^*(\mathbf{x}', t')K(\mathbf{x}', t')\} \\ & = \int_V dV' \{iK(\mathbf{x}', t')\psi(\mathbf{x}', t')\}_{t'=0}^\infty \\ & \quad + \frac{1}{2} \int_0^\infty dt' \int_{\partial V} d\mathbf{f}' \cdot \{K(\mathbf{x}', t')\nabla' \psi(\mathbf{x}', t') \\ & \quad - \psi(\mathbf{x}', t')\nabla' K(\mathbf{x}', t')\}, \end{aligned} \quad (2.4)$$

where $L^*(\mathbf{x}, t) = -i\partial_t + \frac{1}{2}\Delta$, and ∂V denotes the surface of the exterior region, consisting of the inner surface S and an outer surface at infinity. This identity holds between the operators L and L^* for arbitrary functions $\psi(\mathbf{x}, t)$ and $K(\mathbf{x}, t)$.

To obtain a boundary-integral representation of the exterior solution in terms of the boundary values g , the function $K(\mathbf{x}', t')$ will now be defined as the Green function $K(\mathbf{x}, t; \mathbf{x}', t')$, satisfying the initial-boundary value problem

$$L^*(\mathbf{x}', t')K(\mathbf{x}, t; \mathbf{x}', t') = \delta^3(\mathbf{x} - \mathbf{x}')\delta(t - t'), \quad (2.5a)$$

$$K(\mathbf{x}, t; \mathbf{x}', \infty) = 0, \quad (2.5b)$$

$$\partial_{n'} K(\mathbf{x}, t; \mathbf{x}', t') = 0, \quad (2.5c)$$

$$\{K\partial_{n'}\psi - \psi\partial_{n'}K\}|_{|\mathbf{x}'| \rightarrow \infty} = 0. \quad (2.5d)$$

Using these properties for K , and noting that the exterior solution ψ satisfies Eqs. (2.1) and (2.3), there follows, from Eq. (2.4),

$$\psi(\mathbf{x}, t) = \frac{1}{2} \int_0^\infty dt' \int_S dS' K(\mathbf{x}, t; \mathbf{x}'_s, t')g(\mathbf{x}'_s, t'). \quad (2.6)$$

The surface integral vanishes at the outer surface, and at the inner surface $d\mathbf{f}' = -\mathbf{n}'dS'$. Evaluating this solution on the boundary S yields

$$f(\mathbf{x}_s, t) = \frac{1}{2} \int_0^\infty dt' \int_S dS' K(\mathbf{x}_s, t; \mathbf{x}'_s, t')g(\mathbf{x}'_s, t'). \quad (2.7)$$

In general this boundary condition is nonlocal in space and time. The boundary value of the wave function at the surface point \mathbf{x}_s at time t is related to the normal derivatives of the wave function at all surface points \mathbf{x}'_s at all previous times t' . The determination of the Green function $K(\mathbf{x}_s, t; \mathbf{x}'_s, t')$ remains the basic problem to be solved.

B. One-dimensional half-space

For a one-dimensional half-space, $|x| > |x_s|$, the Green function K is a simple modification of the familiar free-particle Green function for an unbounded region. According

to Eq. (2.5), it is identically zero for $t' > t$. It may therefore be calculated by considering a Laplace transformation in time,

$$\hat{K}(x, t; x', \omega) = \int_{-\infty}^{\infty} dt' K(x, t; x', t') e^{i\omega t'}, \quad (2.8a)$$

$$K(x, t; x', t') = \frac{1}{2\pi} \int_C d\omega \hat{K}(x, t; x', \omega) e^{-i\omega t'}. \quad (2.8b)$$

The Laplace transform (2.8a) converges at the upper integration limit $t' \rightarrow \infty$ because of the initial condition (2.5b). At the lower integration limit, convergence is achieved by defining ω in the complex half-plane $\text{Im}(\omega) < c$ below all the singularities of $\hat{K}(x, t; x', \omega)$. The integration contour C of the inverse Laplace transform (2.8b) has to be chosen within this half-plane parallel to the real axis. Applying the Laplace transformation to Eq. (2.5a) with the initial condition (2.5b) yields

$$\partial_x^2 \hat{K} - 2\omega \hat{K} = 2e^{i\omega t} \delta(x - x'). \quad (2.9)$$

The particular solution satisfying the boundary conditions (2.5c) and (2.5d) is readily found to be

$$\hat{K} = \frac{-i}{k} e^{i\omega t} \{e^{ik|z'|+z|} + e^{ik|z'-z|}\}, \quad (2.10)$$

where $z = x - x_s$, $z' = x' - x_s$, and $k = i\sqrt{2\omega}$. The domain of convergence of \hat{K} is the whole half-plane $\text{Im}(\omega) < 0$ and the k branch has to be chosen such that $\text{Im}(k) > 0$ for $\text{Im}(\omega) < 0$. The inverse Laplace transform can be evaluated along the contours shown in Fig. 1(a). For $t' > t$, the solution vanishes, and the initial condition $K(x, t; x', \infty) = 0$ is therefore satisfied. This can be seen by deforming the contour C toward ∞ in the lower ω plane, where the integrand becomes zero. For $t' < t$, the contour integral can be evaluated by deforming the contour C towards ∞ in the upper ω plane. The deformed contour consists of the three sections C_1 , C_2 , and C_3 , indicated in Fig. 1. Along C_1 the phase $\text{Re}(\omega)(t' - t)$ becomes rapidly oscillating as $|\text{Re}(\omega)| \rightarrow \infty$. This contribution can be omitted because of the subsequent time integration in Eq. (2.7). Along the path C_2 the integrand vanishes, and the integral becomes zero. The Green function is therefore determined by the path C_3 around the branch cut along the positive imaginary axis. This integration is performed in the k plane along the contour \tilde{C}_3 , as indicated in Fig. 1(b). Noting that $d\omega = -k dk$, one finds

$$\begin{aligned} K(x, t; x', t') &= \Theta(t - t') \frac{i}{2\pi} \\ &\times \int_{\tilde{C}_3} dk e^{-(i/2)k^2(t-t')} (e^{ik|z'+z|} + e^{ik|z'-z|}) \\ &= \frac{-i\Theta(t-t')}{\sqrt{2\pi i(t-t')}} \\ &\times (e^{(i/2)(z'+z)^2/(t-t')} + e^{(i/2)(z'-z)^2/(t-t')}). \end{aligned} \quad (2.11)$$

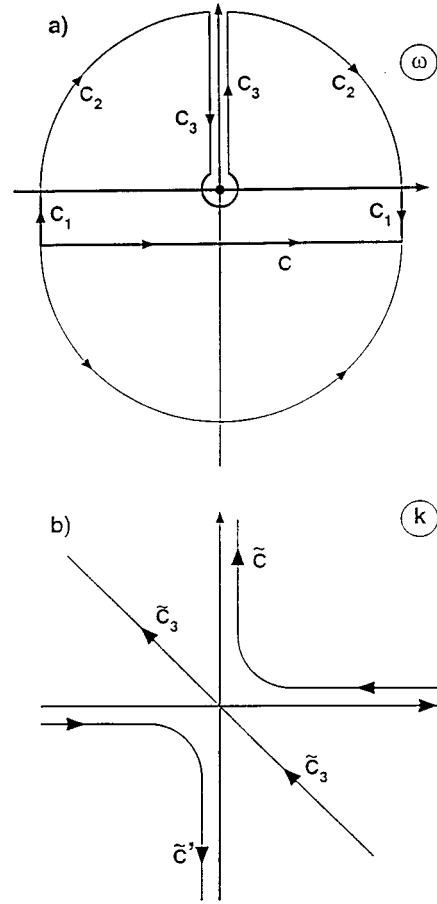


FIG. 1. (a) The integration contour C is defined in the lower ω plane. It is deformed toward infinity in the lower half-plane for $t' > t$ and in the upper half-plane for $t' < t$. Only the path C_3 around the branch cut on the imaginary axis contributes to the Green function. (b) Corresponding contours in the k plane for the branches $k = i\sqrt{2\omega}$ (\tilde{C}) and $k = -i\sqrt{2\omega}$ (\tilde{C}'), and for the mapping \tilde{C}_3 of the integration path C_3 .

The radiation condition (2.7) at the end point x_s of the one-dimensional half-space now assumes the final forms

$$f(x_s, t) = -i \int_0^t dt' \frac{g(x_s, t')}{\sqrt{2\pi i(t-t')}}, \quad (2.12a)$$

$$g(x_s, t) = -2 \int_0^t dt' \frac{\partial_t f(x_s, t')}{\sqrt{2\pi i(t-t')}}. \quad (2.12b)$$

The inverse relationship (2.12b) is obtained by noting that $\partial_x \psi(x, t)$ is also a solution of the one-dimensional Schrödinger equation with the boundary values $\partial_x \psi(x_s, t) = g(x_s, t)$, $\partial_x(\partial_x \psi(x_s, t)) = -2i\partial_t \psi(x_s, t) = -2i\partial_t f(x_s, t)$. Integral-boundary conditions of this type also occur in heat-flow problems, where they constitute a familiar boundary constraint between the temperature and the heat flow [25]. The important fact we wish to emphasize is the possibility of truncating numerical solutions with these relations.

For comparison with the R -matrix Floquet theory, it may be of interest to evaluate the present boundary conditions for Floquet solutions of the form

$$f(t) = e^{-iEt} \sum_n \varphi_n e^{-in\omega t}, \quad g(t) = e^{-iEt} \sum_n \pm \partial_x \varphi_n e^{-in\omega t}, \quad (2.13)$$

where the upper sign corresponds to the asymptotic region $x > 0$, and the lower sign to $x < 0$. Inserting Eq. (2.13) into Eq. (2.12a), one obtains the boundary conditions

$$\varphi_n = \frac{1}{2} \hat{K}(E + n\omega) \partial_x \varphi_n,$$

$$\hat{K}(\Omega) = \pm \int_{-\infty}^{\infty} d\tau \frac{-2i\Theta(\tau)}{\sqrt{2\pi i\tau}} e^{i\Omega\tau} = \frac{2}{\pm i\sqrt{2\Omega}} \quad (2.14)$$

for the expansion coefficients. These may be viewed as an R -matrix equation, corresponding to the simple case where the R matrix is diagonal and the channel functions are plane waves with wave numbers $k_n = \pm \sqrt{2(E + n\omega)}$.

C. Region exterior to a three-dimensional sphere

In the three-dimensional case, the Green function will depend in general on the shape of the surface S . Since the boundary of the interior region may be chosen for convenience, the simplest case of a spherical surface will be assumed. To derive the Green function for the region exterior to a sphere with radius R , Eq. (2.5a) is rewritten in spherical coordinates (r, ϑ, φ) as

$$\begin{aligned} & \left(-2i\partial_{r'} + \frac{1}{r'} \partial_{r'}^2 r' - \frac{L'^2}{r'^2} \right) K \\ &= \delta(t-t') \frac{2}{r'^2} \delta(r-r') \delta(\varphi-\varphi') \\ & \quad \times \delta[\cos(\vartheta) - \cos(\vartheta')], \end{aligned} \quad (2.15)$$

with the angular-momentum operator $L = -i\mathbf{r} \times \nabla$. Expanding angle dependences with respect to spherical harmonics $Y_l^m(\vartheta, \varphi)$, the Green function can be represented in the form

$$K = R^{-2} \sum_{l=0}^{\infty} \sum_{m=-l}^{+l} Y_l^m(\vartheta, \varphi) K_l(r, t; r', t') Y_l^m(\vartheta', \varphi')^*. \quad (2.16)$$

It is noted that $Y_l^m(\vartheta, \varphi)$ and $Y_l^m(\vartheta', \varphi')$ occur with the same mode numbers because of the corresponding property of the δ function,

$$\begin{aligned} & \delta(\varphi - \varphi') \delta[\cos(\vartheta) - \cos(\vartheta')] \\ &= \sum_{l=0}^{\infty} \sum_{m=-l}^{+l} Y_l^m(\vartheta, \varphi) Y_l^m(\vartheta', \varphi')^*. \end{aligned} \quad (2.17)$$

From expansion (2.16) it follows that the partial-wave amplitudes

$$\begin{aligned} f_{lm}(t) &= \int d\Omega Y_l^m(\vartheta, \varphi)^* f(\vartheta, \varphi, t), \\ g_{lm}(t) &= \int d\Omega Y_l^m(\vartheta, \varphi)^* g(\vartheta, \varphi, t) \end{aligned} \quad (2.18)$$

for definite spherical mode numbers satisfy independent radiation conditions

$$f_{lm}(t) = \frac{1}{2} \int_0^T dt' K_l(R, t; R, t') g_{lm}(t'). \quad (2.19)$$

These are determined by the radial part $K_l(r, t; r', t')$ of the Green function evaluated on the surface $r = r' = R$. The Laplace transform $\hat{K}_l(r, t; r', \omega)$ of $K_l(r, t; r', t')$ is now subject to the equation

$$\left(\partial_{r'}^2 + k^2 - \frac{l(l+1)}{r'^2} \right) r' \hat{K}_l = \frac{2R^2 e^{i\omega t}}{r'} \delta(r-r'), \quad (2.20)$$

where k is defined as in Eq. (2.10). For $r' > r$, the solution corresponding to the boundary condition (2.5d) is given by

$$\hat{K}_l(r, t; r', \omega) = C_l(r, t, \omega) h_l^1(kr'), \quad (2.21)$$

where $h_l^1(\varrho)$ denotes the spherical Bessel function of the third kind [26], and C_l an integration constant. The presence of the δ function in Eq. (2.20) requires a jump discontinuity

$$\begin{aligned} & \partial_{r'}(r' \hat{K}_l)|_{r'+} - \partial_{r'}(r' \hat{K}_l)|_{r'-} = r' \partial_{r'} \hat{K}_l|_{r'+} - r' \partial_{r'} \hat{K}_l|_{r'-} \\ &= \frac{2R^2}{r} e^{i\omega t} \end{aligned} \quad (2.22)$$

at $r = r'$. Being interested only in boundary values, one can take the limits $r \rightarrow R$ and $r' \rightarrow R$, while using the solution (2.21) on the side $R+$ and the boundary condition (2.5c) on the side $R-$. This procedure determines the constant $C_l(R, t, \omega)$, yielding

$$\hat{K}_l(R, t; R, \omega) = \frac{2}{k} \frac{h_l^1}{\frac{d}{d\varrho} h_l^1} \Bigg|_{\varrho=kR} e^{i\omega t}. \quad (2.23)$$

Calculating the inverse of the Laplace transform (2.23), the general solution for the radiation conditions is obtained. In practice, however, it may be sufficient to consider an asymptotic expansion of the radiation conditions for sufficiently large R . Restricting attention to the leading term in this expansion,

$$h_l^1(\varrho) \rightarrow \varrho^{-1} e^{i[\varrho - (\pi/2)(l+1)]},$$

$$\hat{K}_l(R, t; R, \omega) \rightarrow \frac{-2i}{k} e^{i\omega t}, \quad K_l(R, t; R, t') \rightarrow \frac{-2i\Theta(t-t')}{\sqrt{2\pi i(t-t')}}, \quad (2.24)$$

the Green function K_l becomes independent of the mode number l , and one recovers the one-dimensional result at each surface point on the sphere:

$$f(\vartheta, \varphi, t) = -i \int_0^t dt' \frac{g(\vartheta, \varphi, t')}{\sqrt{2\pi i(t-t')}}. \quad (2.25)$$

In this limit, the boundary condition is local in space but it still contains memory effects in time.

D. Finite difference representation

Having established the radiation conditions at the boundaries of the interior region, the method for truncating numerical solutions with these conditions will now be described. At present, we restrict attention to one-dimensional TDSE calculations. Such calculations can be performed with a well-known algorithm due to Goldberg, Schey, and Schwartz [27]. It is based on the Crank-Nicolson difference scheme [28] and an efficient solution method for tridiagonal matrices. The latter is also known as the LU decomposition method into lower and upper triangular matrices.

The boundary conditions (2.12) have a square-root singularity in the kernel at the end point t , where the boundary values are to be determined. This singularity makes direct evaluations by numerical quadrature methods quite cumbersome. It is therefore advantageous to remove the singularity from the boundary condition before making finite-difference approximations. This approach leads to a discrete form, which is both simple and accurate.

Performing a partial integration in Eq. (2.12) and assuming the initial values $g(x_s, 0) = \partial_t f(x_s, 0) = 0$, one gains the simpler representations

$$f(x_s, t) = \frac{-2i}{\sqrt{2\pi i}} \int_0^t dt' \sqrt{t-t'} \partial_{t'} g(x_s, t'), \quad (2.26a)$$

$$g(x_s, t) = \frac{-4}{\sqrt{2\pi i}} \int_0^t dt' \sqrt{t-t'} \partial_{t'}^2 f(x_s, t'), \quad (2.26b)$$

which can be handled more easily. The second form will be preferred in the following because of the absence of a mixed second derivative.

The wave function $\psi(x, t)$ is now replaced by a finite-difference representation ψ_j^v at the grid points $x = x_j$ and $t = t^v$, being equally spaced by the intervals δx and δt , respectively. If the boundary x_s is assumed to be centered between the last two grid points x_J and x_{J-1} , where $|x_J| > |x_{J-1}|$, the boundary values $f(x_s, t^v)$ and $g(x_s, t^v)$ can be represented as

$$f^v \rightarrow \frac{\psi_J^v + \psi_{J-1}^v}{2}, \quad g^v \rightarrow \frac{\psi_J^v - \psi_{J-1}^v}{\delta x}. \quad (2.27)$$

Furthermore, the integral (2.26b) can be replaced by a sum formula of the general form

$$\int_0^t dt' F(t') \rightarrow \sum_{\nu=0}^{n+1} \delta t a^\nu F^\nu, \quad (2.28)$$

where the numerical coefficients a^ν depend on the specific quadrature rule. Since the time interval δt is small, one may simply choose the trapezoidal rule. Noting that the integrand vanishes at both end points this corresponds to setting $a^\nu = 1$.

With these substitutions, the finite-difference representation of the boundary condition (2.26b) is found to be

$$\left(1 - \frac{1}{2}A^n\right)\psi_J^{n+1} - \left(1 + \frac{1}{2}A^n\right)\psi_{J-1}^{n+1} = B^n, \quad (2.29)$$

where

$$A^\nu = c_0 a^\nu \frac{\delta x}{\sqrt{\delta t}}, \quad c_0 = \frac{-4}{\sqrt{2\pi i}} = \frac{2(i-1)}{\sqrt{\pi}},$$

$$B^n = A^n(-2f^n + f^{n-1}) + \sum_{\nu=0}^{n-1} A^\nu K^\nu,$$

$$K^\nu = \sqrt{n+1-\nu}(f^{\nu+1} - 2f^\nu + f^{\nu-1}).$$

The solution is assumed to be given up to the time t^n , while t^{n+1} represents the current time step to be solved. Boundary conditions of this form maintain the tridiagonal matrix structure of the Crank-Nicolson algorithm, and can therefore be treated, from the computational viewpoint, without additional complications.

Truncating the numerical solution in space by using the radiation conditions (2.29), one has to pay some price by summing up the boundary values in time. However, in all there results a significant reduction of computation time, as can be seen from the following estimate. The CPU time required for TDSE calculations with radiation conditions can be estimated by

$$t_1 = \alpha J L + \beta(L + L^2) + \gamma, \quad \alpha = 4.1 \times 10^{-7} \text{ min}, \\ \beta = 3.2 \times 10^{-8} \text{ min}, \quad \gamma = 0.18 \text{ min}, \quad (2.30)$$

where L is the number of time steps and J the number of spatial grid points. The values of the coefficients α , β , and γ have been measured with our code, and they depend on the specific implementation. The first term corresponds to the inversion of the tridiagonal matrix of the difference scheme, which takes $O(J)$ operations at each time step. The second term accounts for computing the boundary conditions, which takes $O(\sum_{n=0}^L n) = O[L(L+1)/2]$ operations. Computation times needed before and after the time integration are expressed by the third term. If rigid boundaries are used instead, the second term can be omitted; however, J has to be chosen to be much larger. During the computation time $L \delta t$ the wave function will spread a distance $k_m L \delta t$ to both sides of the atom, where $k_m = \sqrt{2} \omega_m$ corresponds to the velocity of the maximum photon order. Setting, therefore,

$$J \delta x = 2(k_m L \delta t), \quad \frac{\delta t}{\delta x} \approx \frac{k_m}{\omega_m}, \quad (2.31)$$

one obtains $J \approx 4L$. Using this value in Eq. (2.30), the CPU time required with rigid boundaries can be estimated by

$$t_2 = 4\alpha L^2 + \gamma. \quad (2.32)$$

For $L \rightarrow \infty$, the ratio of computation times is given by

$$\frac{t_2}{t_1} = \frac{4\alpha}{\beta} \approx 40. \quad (2.33)$$

In accordance with this estimate, our calculations with large numbers of time steps are approximately one order of magnitude faster than corresponding calculations with rigid boundaries. The limit of large L is reached for either long computation times (several tens of light periods) or for small

time steps. Such small time steps arise for ATI calculations with large ponderomotive potentials.

III. NUMERICAL RESULTS

To validate the numerical procedure, we have performed one-dimensional TDSE calculations for strong-field photoionization. The nonrelativistic interaction of a one-electron atom with an electromagnetic wave is governed by the Schrödinger equation

$$i\partial_t\psi(\mathbf{x},t)=H\psi(\mathbf{x},t), \quad H=-\frac{1}{2}\Delta+V(\mathbf{x})+\mathbf{x}\cdot\mathcal{E}(t) \quad (3.1)$$

for the wave function $\psi(\mathbf{x},t)$. $V(\mathbf{x})$ denotes the atomic potential, and the electromagnetic wave is described within the electric-dipole approximation by a time-dependent electric field $\mathcal{E}(t)$.

To apply the free-particle radiation conditions derived above, it is necessary to choose a representation where the interaction is localized and the electron becomes asymptotically free. The effect of a spatially constant acceleration by the electric field is equivalent to an accelerated coordinate frame. The transformation to the accelerated frame is known as the Kramers-Henneberger transformation [29,30],

$$\tilde{\psi}(\mathbf{x},t)=e^{-i\dot{\xi}(t)\cdot\mathbf{x}+(i/2)\int_0^t\dot{\xi}^2(t')dt'}\psi(\mathbf{x},t), \quad (3.2a)$$

$$\Phi(\mathbf{u},t)=\tilde{\psi}[\mathbf{u}+\boldsymbol{\xi}(t),t]. \quad (3.2b)$$

Here $\Phi(\mathbf{u},t)$ is the transformed wave function, and $\boldsymbol{\xi}(t)$ has to be chosen as a solution of the classical equation of motion, $\ddot{\boldsymbol{\xi}}(t)=-\mathcal{E}(t)$. The unitary transformation (3.2a) transforms from the length gauge to the velocity gauge. The subsequent coordinate transformation $\mathbf{u}=\mathbf{x}-\boldsymbol{\xi}(t)$ eliminates the effect of the electric field on a free electron ($V=0$). The latter can also be viewed as a second unitary transformation by noting that

$$\Phi(\mathbf{u},t)=e^{i\boldsymbol{\xi}\cdot\mathbf{p}}\tilde{\psi}(\mathbf{u},t), \quad \mathbf{p}=-i\nabla. \quad (3.3)$$

As a result of these transformations, the Schrödinger equation for the wave function $\Phi(\mathbf{u},t)$ is found to be

$$i\partial_t\Phi=\left\{-\frac{1}{2}\Delta+V[\mathbf{u}+\boldsymbol{\xi}(t)]\right\}\Phi. \quad (3.4)$$

The interaction with the electric field is now described by a time-dependent displacement of the atomic potential. If r denotes the range of the potential, the extent of the interaction region will be of the order $r+|\boldsymbol{\xi}|$. Outside this region the electron can be described by the free-particle equation (2.1).

In our one-dimensional calculations, the atom is modeled by the potential

$$V(x)=-\frac{1}{\cosh^2(x)}. \quad (3.5)$$

It has only a single bound state

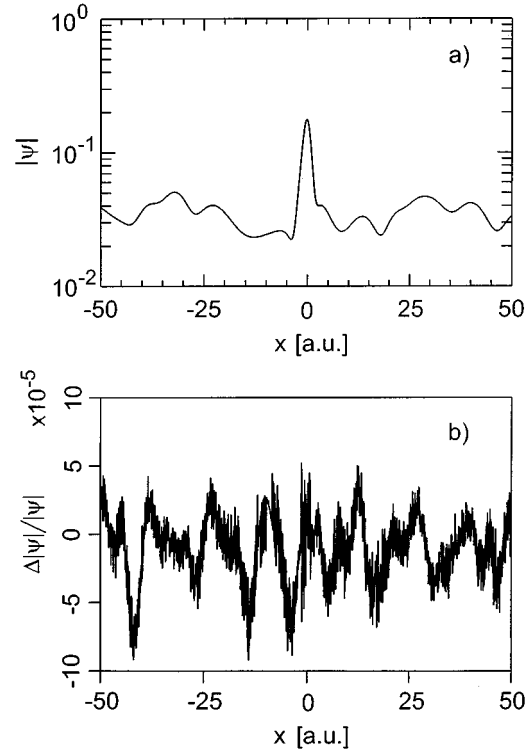


FIG. 2. (a) Numerical solution $|\psi(x)|$ after 16 light periods for $\mathcal{E}_0=0.1$ and $\omega=0.2$. (b) Relative error between the truncated solution with boundaries at $x=\pm 50$ and the complete solution with rigid boundaries at $x=\pm 1000$.

$$\psi_0(x,t)=\frac{1}{\sqrt{2}\cosh(x)}e^{-iE_0t}, \quad E_0=-0.5, \quad (3.6)$$

which is taken as the initial state at $t=0$ in all calculations. The electric field is assumed as a purely monochromatic wave,

$$\mathcal{E}(t)=\mathcal{E}_0\sin(\omega t), \quad (3.7)$$

with a constant amplitude \mathcal{E}_0 and frequency ω . Since detailed one-dimensional calculations have already been reported [7], we restrict the discussion to a few examples, illustrating the computational accuracy of the method, and the calculation of asymptotic properties by the truncated solution.

A. Wave function

A numerical solution for the magnitude of the wave function after 16 light periods can be seen in Fig. 2(a). It corresponds to the parameters $\mathcal{E}_0=0.1$ and $\omega=0.2$. The present boundary conditions (2.29) have been imposed at $x=\pm 50$. One can recognize the bound state near $x=0$ as well as the free part of the wave function extending up to the boundaries. For comparison, the complete solution has also been calculated by using a large grid with conventional rigid boundary conditions at $x=\pm 1000$. The differences between the full and truncated solutions are too small to be noticeable in the graphical representation of Fig. 2(a). Therefore the relative error $\Delta|\psi|/|\psi|$ between the two solutions has been calculated explicitly, and represented in Fig. 2(b) as a func-

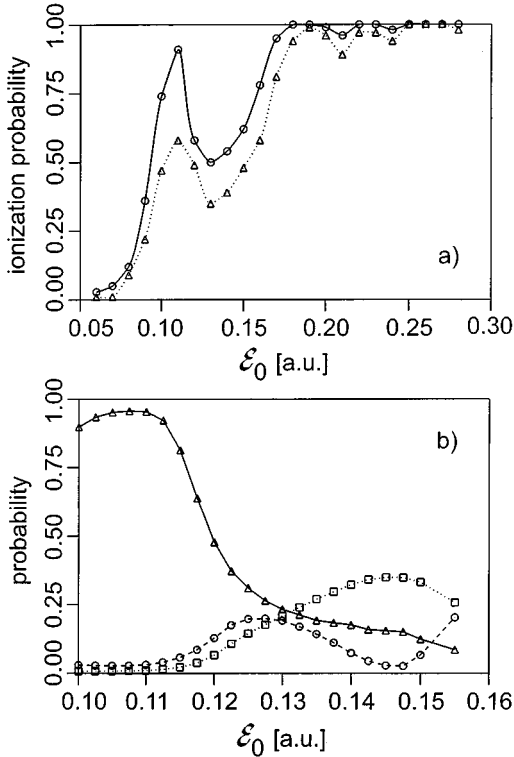


FIG. 3. (a) Variation of the ionization probability with the field strength after four (dotted line) and eight (solid line) light periods for a monochromatic field with frequency $\omega=0.2$. (b) Branching ratios for the photon orders 3 (Δ), 4 (\circ), and 5 (\square) for the same parameters.

tion of x . It can be seen that the error is of the order of 10^{-5} , such that the present truncation method can be considered highly accurate. Varying computation times, we have also convinced that the size of the error does not grow with time.

B. Ionization probability

The truncated solution is also sufficient to calculate ionization probabilities and energy spectra. In our calculations the ionization probability has been defined as the probability

$$p_{\text{ion}}(t) = 1 - \left| \int_{-\infty}^{\infty} \psi_0^*(x,t) \psi(x,t) dx \right|^2 \quad (3.8)$$

that the electron does not occupy the bound state of the unperturbed atom. Strictly speaking, this definition is only meaningful before and after the interaction with the laser field. During the laser pulse, probability (3.8) is slightly modulated at twice the laser frequency, assuming a minimum value at each zero of the electric field. However, this modulation is small, and definition (3.8) can be taken as a good estimate of the time-dependent ionization probability. In the following, the ionization probability calculated after a few light periods will be discussed.

Figure 3(a) shows the ionization probability as a function of the field amplitude for a fixed frequency $\omega=0.2$. The two curves have been obtained after four (dotted) and eight (solid) light periods, showing similar variations with the field

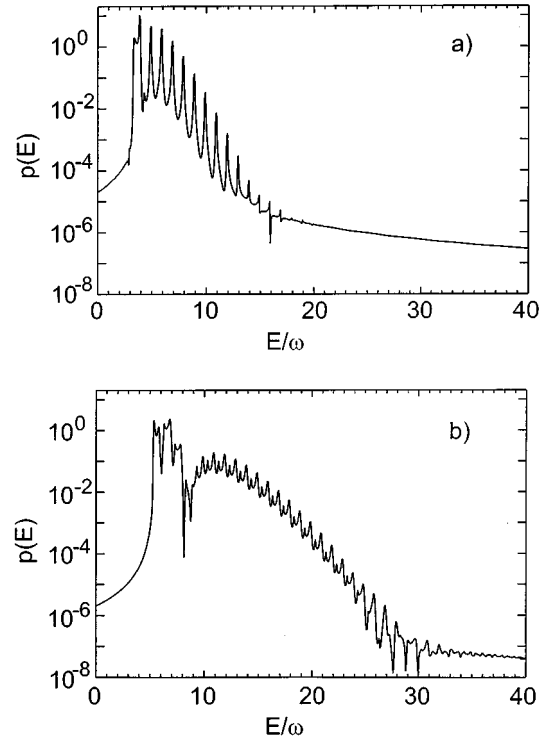


FIG. 4. Energy spectrum after 16 light periods for a monochromatic field with frequency $\omega=0.2$. (a) Regular ATI spectrum for $\mathcal{E}_0=0.16$. The photon order 3 is suppressed by channel closing. (b) ATI spectrum with additional scattering peaks in over-the-barrier ionization ($\mathcal{E}_0=0.3$).

strength. In the figure, one can observe the transition from three- to four-photon ionization due to the effect of channel closing. By energy conservation, n -photon absorption will be suppressed if

$$n\omega < |E_0| + U_p, \quad U_p = \frac{\mathcal{E}_0^2}{4\omega^2}. \quad (3.9)$$

The ionization energy $|E_0|$ is enhanced by the ponderomotive potential U_p . From Eq. (3.9), there follow the threshold fields $\mathcal{E}_0=0.126$ for $n=3$ and $\mathcal{E}_0=0.219$ for $n=4$. This simple estimate is in good accordance with the calculated ionization minima around these values. Actually, there is no sharp threshold because of the finite linewidth of the transition. The ionization probability into the three lowest photon channels $n=3, 4$ and 5 is shown in more detail in Fig. 3(b). The suppression of the three-photon peak above $\mathcal{E}_0 \approx 0.11$ can be clearly recognized.

C. Energy spectrum

Energy spectra can also be directly calculated from the truncated solution in the Kramers-Henneberger (KH) frame. At a fixed position x_s near the boundary, we take the Fourier transform

$$\hat{\Phi}(x_s, \Omega) = \frac{1}{2\pi} \int_{-\infty}^{\infty} \Phi(x_s, t) e^{i\Omega t} dt \quad (3.10)$$

with respect to time, and define $|\hat{\Phi}(x_s, \Omega)|^2$ as the probability that the electron has the energy Ω at the corresponding boundary. To obtain the total-energy spectra the contributions from both boundaries have to be added. With increasing computation time a very high-energy resolution is gained. After N light periods one has $\delta\Omega/\omega \approx 1/N$. Energy spectra calculated alternatively with the full asymptotic solution at a fixed time by a spatial Fourier transform do not show appreciable differences.

The energy Ω in the KH frame represents the kinetic energy in the absence of the laser field. The total absorbed energy is given by

$$E = |E_0| + U_p + \Omega, \quad (3.11)$$

where the ionization energy is approximated by Eq. (3.9). We have represented the energy spectra as a function of E/ω , since regular ATI peaks are expected near the energies $E = n\omega$. Figure 4(a) shows a series of ATI peaks, obtained for the parameters $\omega = 0.2$ and $\mathcal{E}_0 = 0.16$, after 16 light periods. Note that the three-photon peak is already suppressed at this intensity. If the field strength is further increased, one enters the regime of over-the-barrier ionization. To suppress the potential barrier below the binding energy E_0 , the critical field strength $\mathcal{E}_c \approx 0.22$ has to be exceeded. In this regime, we have observed an additional peak series in some cases. An example is shown in Fig. 4(b), corresponding to the parameters $\omega = 0.2$ and $\mathcal{E}_0 = 0.3$. While the regular ATI series appears at the energies $E = n\omega$, the peaks of the additional series can be recognized at the energies $\Omega = n\omega$. In the present representation, the lowest-order peak ($n = 0$) occurs at $E/\omega \approx 5.3$. Since the absorbed energies $n\Omega$ are independent of the ionization energy, this peak series may be regarded as a free-free multiphoton transition due to the scat-

tering of an oscillating part of the wave function by the atomic potential. It is noted, that a similar peak series has been predicted before in theoretical work based on a δ -function potential [31].

IV. CONCLUSIONS

In the present work, we have derived exact radiative boundary conditions to truncate the numerical solution of the TDSE at the boundaries of the numerical grid. An explicit finite-difference expression for one-dimensional calculations has been gained. The method has been validated in the context of strong-field photoionization. Thereby the truncated wave function has been found to be in excellent agreement with the corresponding full solution. Both ionization probabilities and energy spectra have been obtained by this method.

The present calculations have successfully demonstrated advantages of radiation conditions in one-dimensional ATI calculations. While useful insight into basic ATI features can be gained from a one-dimensional model, it is clearly too restricted to allow for quantitative comparisons with experiments. It is therefore hoped that the present computational method also will prove adequate for three-dimensional calculations. Radiation conditions have been derived for a spherical surface in the Kramers-Henneberger frame. However, their applicability to TDSE calculations for more realistic atoms requires further investigation. These issues will be the subject of a forthcoming work.

ACKNOWLEDGMENT

We wish to acknowledge helpful discussions with B. U. Felderhof and G. Herziger. This work has been supported by the European Commission through the TMR Network SILASI, Contract No. ERBFMRX-CT96-0043 and by the Deutsche Forschungsgemeinschaft, Bonn.

-
- [1] *High-Order Processes in Atoms*, edited by K. Kulander and A. L'Huillier, Special Issue of J. Opt. Soc. Am. B **7**, 403 (1990).
- [2] J. H. Eberly, J. Javanainen, and K. Rzażewski, Phys. Rep. **204**, 331 (1991).
- [3] A. L'Huillier *et al.*, Phys. Rev. A **46**, 2778 (1992).
- [4] A. Goldberg and B. W. Shore, J. Phys. B **11**, 3339 (1978).
- [5] J. Javanainen, J. H. Eberly, and Q. Su, Phys. Rev. A **38**, 3430 (1988).
- [6] Q. Su, J. H. Eberly, and J. Javanainen, Phys. Rev. Lett. **64**, 862 (1990).
- [7] W. G. Greenwood and J. H. Eberly, Phys. Rev. A **43**, 525 (1991).
- [8] R. Grobe and J. H. Eberly, Phys. Rev. Lett. **68**, 2905 (1992).
- [9] K. Burnett, P. L. Knight, B. R. M. Piraux, and V. C. Reed, Phys. Rev. Lett. **66**, 301 (1991).
- [10] K. C. Kulander, Phys. Rev. A **35**, 445 (1987).
- [11] K. C. Kulander and B. W. Shore, J. Opt. Soc. Am. B **7**, 502 (1990).
- [12] K. C. Kulander, K. J. Schafer, and J. L. Krause, Phys. Rev. Lett. **66**, 2601 (1991).
- [13] K. C. Kulander, K. J. Schafer, and J. L. Krause, Int. J. Quantum Chem. **25**, 415 (1991).
- [14] J. Purvis *et al.*, Phys. Rev. Lett. **71**, 3943 (1993).
- [15] A. Sommerfeld, Jber. D.M.V. Leipzig **21**, 309 (1912).
- [16] C. Leforestier and R. E. Wyatt, J. Chem. Phys. **78**, 2334 (1983).
- [17] R. Kosloff and D. Kosloff, J. Comput. Phys. **63**, 363 (1986).
- [18] D. Neuhauser and M. Baer, J. Chem. Phys. **90**, 4351 (1989).
- [19] R. W. Heather, Comput. Phys. Commun. **63**, 446 (1991).
- [20] C. W. McCurdy and C. K. Stroud, Comput. Phys. Commun. **63**, 323 (1991).
- [21] M. Pont, D. Proulx, and R. Shakeshaft, Phys. Rev. A **44**, 4486 (1991).
- [22] B. Piraux and R. Shakeshaft, Phys. Rev. A **49**, 3903 (1994).
- [23] J. R. Hellums and W. R. Frensley, Phys. Rev. B **49**, 2904 (1994).
- [24] E. Zauderer, *Partial Differential Equations of Applied Mathematics* (Wiley, New York, 1983), p. 353.
- [25] L. D. Landau and E. M. Lifshitz, *Fluids Mechanics* (Pergamon, New York, 1959), p. 200.

- [26] *Handbook of Mathematical Functions*, edited by M. Abramowitz and I. A. Stegun (Dover, New York, 1965), p. 437.
- [27] A. Goldberg, H. M. Schey, and J. L. Schwartz, *Am. J. Phys.* **35**, 177 (1967).
- [28] J. Crank and P. Nicolson, *Proc. Cambridge Philos. Soc.* **43**, 50 (1947).
- [29] H. A. Kramers, *Collected Scientific Papers* (North-Holland, Amsterdam, 1956), p. 262.
- [30] W. C. Henneberger, *Phys. Rev. Lett.* **21**, 838 (1968).
- [31] F. H. M. Faisal and P. Scanzano, *Phys. Rev. Lett.* **68**, 2909 (1992).